



UNIVERSITY OF LEEDS

This is a repository copy of *Bubble formation in freezing droplets*.

White Rose Research Online URL for this paper:

<https://eprints.whiterose.ac.uk/155096/>

Version: Accepted Version

---

**Article:**

Chu, F, Zhang, X, Li, S et al. (4 more authors) (2019) Bubble formation in freezing droplets. *Physical Review Fluids*, 4 (7). 071601(R). ISSN 2469-990X

<https://doi.org/10.1103/physrevfluids.4.071601>

---

© 2019 American Physical Society. This is an author produced version of a paper published in *Physical Review Fluids*. Uploaded in accordance with the publisher's self-archiving policy.

**Reuse**

Items deposited in White Rose Research Online are protected by copyright, with all rights reserved unless indicated otherwise. They may be downloaded and/or printed for private study, or other acts as permitted by national copyright laws. The publisher or other rights holders may allow further reproduction and re-use of the full text version. This is indicated by the licence information on the White Rose Research Online record for the item.

**Takedown**

If you consider content in White Rose Research Online to be in breach of UK law, please notify us by emailing [eprints@whiterose.ac.uk](mailto:eprints@whiterose.ac.uk) including the URL of the record and the reason for the withdrawal request.



[eprints@whiterose.ac.uk](mailto:eprints@whiterose.ac.uk)  
<https://eprints.whiterose.ac.uk/>

# Bubble formation in freezing droplets during icing and condensation frosting

Fuqiang Chu, Shaokang Li, Haichuan Jin, Jun Zhang, Dongsheng Wen\*

School of Aeronautic Science and Engineering, Beihang University, Beijing 100191, China

## Abstract

Freezing of water droplets on solid surfaces has been focused for many years, but there are still some significant mechanisms unrevealed. Here, we reported that bubble formation phenomenon always occurs in freezing droplets, regardless of millimeter sessile droplets or micro-scale condensed droplets. In the second stage of freezing (the first stage is nucleation), air dissolved in liquid water is separated out in the ice front, forming many isolated bubbles. As the ice front grows upwards quickly, these old bubbles are entrapped in ice before they could float up and new bubbles form. We also proposed a theoretical model to elucidate the relationship between bubble formation and its influencing factors, mainly including the gas solubility, the subcooled degree, the freezing time, as well as the droplet size and the surface contact angle. Due to the bubble formation, the final ice droplet is actually a porous media rather than solid ice. According to our measurements, the bubble volume fraction in an ice droplet is as large as 6%. These results may bring some new changes in anti-icing/deicing techniques, such as more accurate assessment of ice quantity and ice adhesion.

Icing phenomenon is ubiquitous in nature and industry. When the ambient temperature is below the freezing point, icing of a water droplet occurs. In most instances, icing is undesired and causes numerous problems, such as reduction of the crop production in agriculture [1], threaten to the flight safety in aviation [2], and heat transfer deterioration in heat exchanger systems [3]. Thus, to avoid the hazards of icing, icing mechanisms and anti-icing technologies have received considerable attentions over the past decades. Researchers have figured out the ice nucleation physics (homogeneous nucleation at liquid-free interface or heterogeneous nucleation at solid-liquid interface) under humidity or gas flow environments [4,5], investigated the freezing front growth and droplet shape evolution features [6,7], and revealed the pointy tip formation mechanism at the later stage of icing [8,9]. Some unique phenomena or behaviors during icing like frost halo [10], dry zone [11], droplet trampolining [12], droplet fragmentation and bursting [13,14] are also focused with their mechanism explained perfectly. Besides these studies on icing, many anti-icing methods are proposed to suppress the ice accretion, one of which is the application of nanoengineered surfaces. Researchers fabricated numerous surfaces with various structures and wettability and used them to delay the ice nucleation [15-17], reduce the ice adhesion [18,19], and even self-clean subcooled droplets or melting frost [20-22], and have achieved expected results.

However, there are still some significant phenomena unfocused. For example, although one may have observed tiny bubbles trapped in ice cubes frozen in fridges [23] or big bubbles embedded in natural pond ice [24], nobody really notices and attaches importance to the bubble formation in an icing droplet. Because of the peculiarity of the droplet icing dynamics, bubble formation in a small icing droplet is more fascinating but also more complicated compared with that in bulk ice. In this letter, we conducted icing and condensation frosting experiments and demonstrated that bubble formation phenomenon is universal in icing droplets (the average bubble volume fraction in ice droplets is up to 6%), regardless of the millimeter sessile droplets or micro-scale condensed droplets. Via a well-designed re-icing process, we clearly observed the bubble formation in the ice front and explained its mechanism. Then a theoretical model coupled with the droplet freezing physics was proposed to elucidate the relationship between the bubble formation and its influencing factors.

In this work, two kinds of Al-based surfaces were used as the experimental surfaces with surface S1 fabricated by the chemical etching-deposition method [25] and surface S2 fabricated by the chemical etching method [26] (See Fig. S1 in supplementary materials [27] (为支撑材料预留) for the two surfaces' SEM images).

At room temperature (20°C), both S1 and S2 are superhydrophobic, but when the test droplets are subcooled under the icing conditions, the two surface CAs decrease. This is mainly due to the capillary condensation and thin water film formation adjacent to the triple phase line [28]. Table 1 shows the detailed CA measurement results for S1 and S2 at both room and subcooled temperatures, where the standard deviations are based on five measurements. Then we conducted icing experiments and condensation frosting experiments (See Fig. S2 in supplementary materials for the schematic of the experimental system). In the icing experiments, we used millimeter sessile droplets (deionized water without degas processing) of 1  $\mu\text{L}$ , 2  $\mu\text{L}$ , and 4  $\mu\text{L}$  volume; in the condensation frosting experiments, the condensed droplets are micro-scale with various sizes. During the experiments, the lab temperature was measured to be  $20.0\pm 1.0^\circ\text{C}$  with a relative humidity range from 20% to 40%. The cold surface temperatures were  $-20.0\pm 0.1^\circ\text{C}$  for surface S1 and  $-15.0\pm 0.1^\circ\text{C}$  for surface S2 (See Fig. S3 in supplementary materials for the temperature and humidity variations during the experiments).

TABLE 1. Experimental surfaces and droplets

Surfaces	CA (20°C)	CA (Subcooled)	Droplets
S1	$159.1\pm 1.6^\circ$	$147.2\pm 1.2^\circ$ ( $-20^\circ\text{C}$ )	Sessile droplets (1 $\mu\text{L}$ , 2 $\mu\text{L}$ , 4 $\mu\text{L}$ ) and condensed droplets
S2	$151.7\pm 1.7^\circ$	$129.0\pm 1.7^\circ$ ( $-15^\circ\text{C}$ )	Sessile droplets (1 $\mu\text{L}$ , 2 $\mu\text{L}$ , 4 $\mu\text{L}$ ) and condensed droplets

Icing of a droplet usually experiences two stages including nucleation/recalescence and freezing, where the former is a very rapid, kinetically controlled process, and the latter is a heat transfer controlled process [4]. Figure 1(a) shows a typical icing phenomenon of a sessile droplet (2  $\mu\text{L}$  droplet on S1) from top-view, where we can see the nucleation/recalescence and the onset of freezing very clearly. What is surprising is that, after the onset of freezing, many tiny bubbles begin to appear, and when the whole droplet is frozen, one can see dense spots distributed on/in the top-view droplet (See supplementary video S1). These spots are bubbles whose size is of 10  $\mu\text{m}$  scale. Figure 1(b) shows the deicing process of the ice droplet in Fig. 1(a) from top-view. From the partial enlarged drawings, one can see many tiny bubbles surrounding or embedded in the unmelted ice cover. Even when the ice melts completely, these bubbles exist for a period (See supplementary video S2). The side-view images in Fig. 1(c) also clearly shows the fast-moving bubbles around the unmelted ice cover (See supplementary video S3). These images in Fig. 1(b) and (c) are strong evidences of the bubble formation in icing droplets.

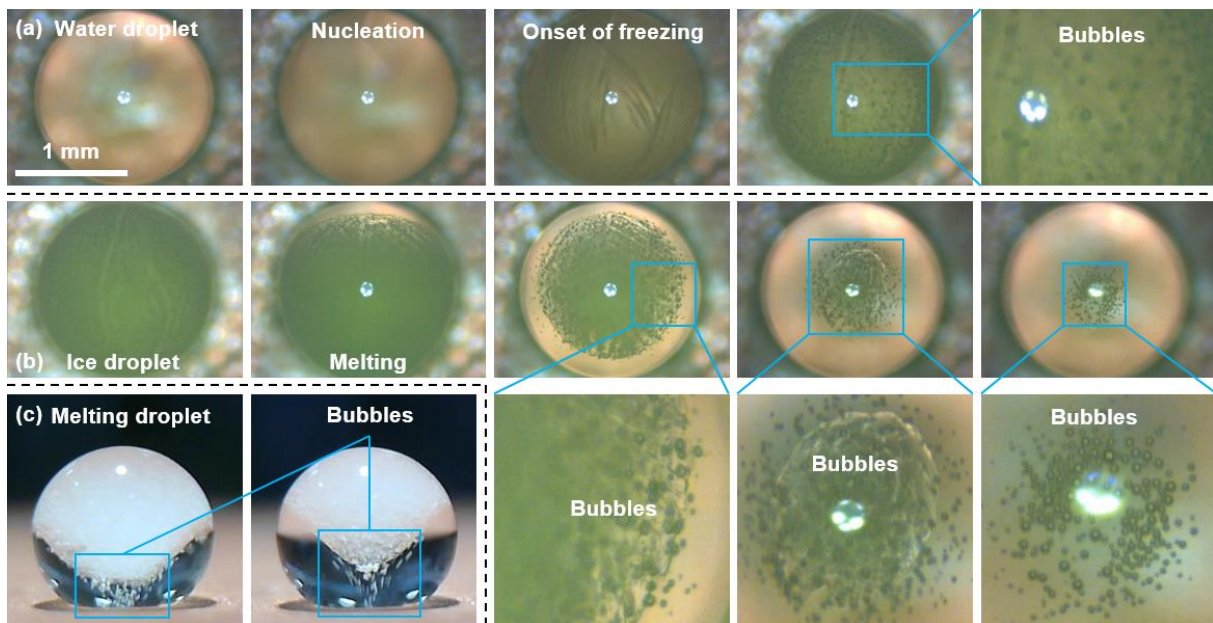


FIG. 1. (a) Direct observation of bubble formation during freezing of a sessile droplet from top-view. In the second stage of freezing, air dissolved in subcooled water droplet dissolves out due to water-ice phase change, forming isolated bubbles of micron scale. The partial enlarged drawing shows these bubbles more clearly. (b) Indirect proof of bubble formation in freezing droplets via observing its melting process of an ice droplet from top-view. From the partial enlarged drawings, one can see many tiny bubbles surrounding or embedded in the unmelted ice cover. Even when the ice melts completely, these bubbles exist for a period. (c) Indirect proof of bubble formation in freezing droplets via observing the melting process from side-view. Many bubbles surround the unmelted ice cover, moving quickly.

Bubble formation not only exists in the process of icing of millimeter sessile droplets, but also occurs in micro-scale condensed droplets during condensation frosting. Figure 2(a) shows the condensation frosting process on surface S1 (See supplementary video S4). From the partial enlarged drawing, one can see the differences between the ice droplets behind the frost front and the water droplet ahead. There are entrapped bubbles (dark blue dots in the images) in the ice droplets, while the water droplets are limpid. Similarly, observe the defrosting droplets shown in Fig. 2(b), the bubbles embedded in the unmelted ice are also proof of the bubble formation in icing droplets during condensation frosting (See supplementary video S5).

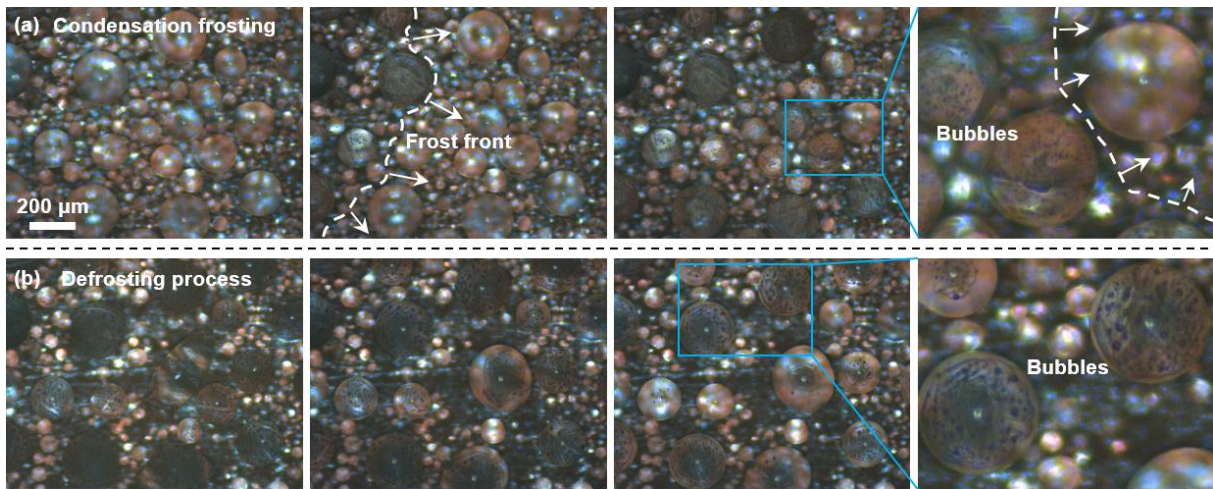


FIG. 2. (a) Direct observation of bubble formation in freezing droplets during condensation frosting. From the partial enlarged drawing, one can see the differences between the ice droplets behind the frost front and the water droplet ahead. Those tiny, dark blue dots are bubbles entrapped in ice droplets. (b) Indirect proof of bubble formation in freezing droplets during condensation frosting via observing the defrosting process. The partial enlarged drawing shows clearly that there are many bubbles (blue dots) embedded in the unmelted ice covers of droplets.

From Figs. 1 and 2, we demonstrated that the bubble formation phenomenon is universal in icing droplets, regardless of the droplet scale, millimeter scale or micro-scale. In addition, we deduced that the bubble formation also exists in the icing process of impacting droplets [29], though we did not conducted related experiments. As known, water can dissolve a certain volume of air (for example, 1000 ml water at 0°C can dissolve about 30 ml air), so when the water solidifies into ice, the dissolved air has to dissolve out, forming bubbles in solid ice. To see the bubble formation in icing droplets more clearly, we designed a re-icing process, which means refreezing a partially melted ice droplet (like those shown in Fig. 1(b) and (c)) before the ice in the droplet melts completely. As mentioned above, the first stage of a pure water droplet icing is nucleation/recalescence, which could make the droplet appear clouding [4]. As a result, it is hard to see how the bubble forms in an icing droplet. However, the re-icing process is different. Because of the existence of ice, the re-icing process does not experience the clouded

recalescence stage, so droplet keeps transparent in the freezing stage. Figure 3(a) shows two images during the re-icing process. As seen, the re-icing droplet is transparent that one can see the ice front clearly, as well as the bubbles separated out from the ice front (See supplementary video S6). Because the rising speed of bubbles is smaller than the ice front speed, old bubbles are entrapped in ice before they could float up and new bubbles form, until the droplet is frozen completely.

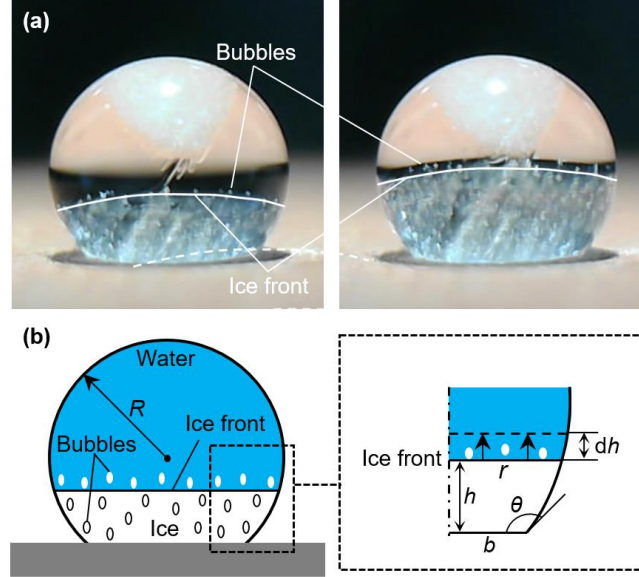


FIG. 3. (a) Bubble formation mechanism determination through a controlled re-icing process of a partially melted ice droplet. During the re-icing process, the unmelted ice provides enough nucleation sites, so heterogeneous nucleation at the solid surface-liquid interface does not occur, and the clouding phenomenon due to recalescence does not appear either. Therefore, the bubble formation mechanism is observed more clearly that bubbles are separated out in the ice front, and as the ice front grows upwards, old bubbles are entrapped in ice before they could float up and new bubbles form, until the droplet is frozen completely. (b) Schematic of bubble formation in freezing droplets. Assuming that the ice front is flat, and the bubble is incompressible and will not spill into the surrounding air. Water evaporation during icing is also neglected. In the schematic,  $h$  is the ice front height,  $dh$  is the moving distance of ice front during  $dt$  time, and  $r$  is the ice front radius;  $R$  is the curvature radius of the droplet,  $b$  is the base radius of the droplet and  $b=R\sin\theta$ , where  $\theta$  is the surface contact angle.

To assess the bubble formation rate and determine its influencing factors, a theoretical model coupled with the droplet icing physics was proposed. In the model, we assume that the ice front is flat, and the bubble is incompressible and will not spill into the surrounding air (the bubble volume is conservative). Water evaporation during icing is also neglected (the water volume is conservative). As shown in Fig. 3(b), after infinitesimal time,  $dt$ , the ice front move up  $dh$ , then solidified water volume,  $dV_{\text{water}}$ , is calculated as

$$dV_{\text{water}} = \nu(1 - \beta)\pi r^2 dh \quad (1)$$

where  $\nu$  is the ratio of ice and water densities;  $\beta$  is the bubble volume fraction in ice, and assume  $\beta$  is constant everywhere;  $r$  is the radius of the ice front. Considering the conservation of water and bubble volumes, bubble volume fraction,  $\beta$ , has a relation with the air solubility in water,  $\alpha$ . That is  $\alpha = \beta/\nu(1 - \beta)$ . So, released bubble volume during  $dt$  time is written as

$$dV_{\text{bubble}} = \left(1 + \frac{1}{\alpha\nu}\right)^{-1} \pi r^2 dh \quad (2)$$

According to literature [30], when assuming the ice front is flat, the relationship between the ice front height,  $h$ ,

and the time,  $t$ , can be derived as  $h = (2B\Delta Tt)^{0.5}$ , where  $B = \lambda_{\text{ice}}/\rho_{\text{ice}}L_m$ ;  $\Delta T$  is the subcooled temperature;  $\lambda_{\text{ice}}$  and  $\rho_{\text{ice}}$  are the thermal conductivity and the density of ice, respectively;  $L_m$  is the latent heat of water solidification. So,

$$\frac{dh}{dt} = \left(\frac{B\Delta T}{2t}\right)^{\frac{1}{2}} \quad (3)$$

According to Marin et al. [8], at the later stage of freezing or for the droplet on hydrophilic surfaces,  $dr^2/dt = -B\Delta T$ . With the boundary condition that  $t=0$ ,  $r=b$ ,  $r^2$  is derived as

$$r^2 = -2B\Delta Tt + b^2 \quad (4)$$

where  $b$  is the base radius of the droplet.  $b$  is also related to the curvature radius of the droplet,  $R$ , and the surface CA,  $\theta$ . That means  $b = R\sin\theta$ . Thus, substituting Eqs. (3) and (4) into Eq. (2) gets the bubble formation rate in icing droplets on hydrophilic surfaces,

$$\frac{dV_{\text{bubble}}}{dt} = \pi \left(1 + \frac{1}{v\alpha}\right)^{-1} \cdot (-2B\Delta Tt + R^2 \sin^2 \theta) \cdot \left(\frac{B\Delta T}{2t}\right)^{\frac{1}{2}} \quad (5)$$

For the droplet on hydrophobic surfaces, a critical time,  $t_{\text{cri}} = R^2 \cos^2 \theta / 2B\Delta T$ , when  $r=R$  should be considered. Thus, the bubble formation rate in icing droplets on hydrophobic surfaces is

$$\frac{dV_{\text{bubble}}}{dt} = \begin{cases} \pi \left(1 + \frac{1}{v\alpha}\right)^{-1} \cdot (2B\Delta Tt + R^2 \sin^2 \theta) \cdot \left(\frac{B\Delta T}{2t}\right)^{\frac{1}{2}}, & t \leq t_{\text{cri}} \\ \pi \left(1 + \frac{1}{v\alpha}\right)^{-1} \cdot (-2B\Delta Tt + 2R^2 - R^2 \sin^2 \theta) \cdot \left(\frac{B\Delta T}{2t}\right)^{\frac{1}{2}}, & t > t_{\text{cri}} \end{cases} \quad (6)$$

According to Eqs. (5) and (6), the bubble formation rate in icing droplet is related to the air solubility,  $\alpha$ , the subcooled temperature,  $\Delta T$ , the droplet curvature radius,  $R$ , the surface CA,  $\theta$ , as well as the time,  $t$ . Figure 4 draws these relations. As Fig. 4(a) shows, the bubble formation rate increases with increasing air solubility (actually, the increasing is approximately linear). Figure 4(a) also shows the variation of the bubble formation rate versus time. On a superhydrophobic surface with a  $150^\circ$  CA, the bubble formation rate first decreases quickly, and then increases slowly until the ice front radius reaches the maximum value. After that, the bubble formation rate continues to decrease until the droplet is frozen completely. From Fig. 4(d), with different CAs, the variations of the bubble formation rate versus time are different. When CA is  $90^\circ$ , the bubble formation rate decreases monotonously; when CA is  $130^\circ$ , the bubble formation rate also decreases but has a turning point. These results are all attributed to the droplet icing physics. Figure 4(b) shows the relation between the bubble formation rate and the subcooled temperature. As seen, the subcooled temperature mainly affects the variation gradient and the location of the turning point (if CA  $> 90^\circ$ ). In addition, it should be noted that, in Fig. 4(b), the areas enclosed between the bubble formation rate curves and the x-axis are equal, which indicates that the subcooled temperature does not influence the total bubble volume. Figure 4(c) shows the relation between the bubble formation rate and the droplet curvature radius. As seen, although these bubble formation rates are different, they are actually self-similar for different droplet curvature radii.

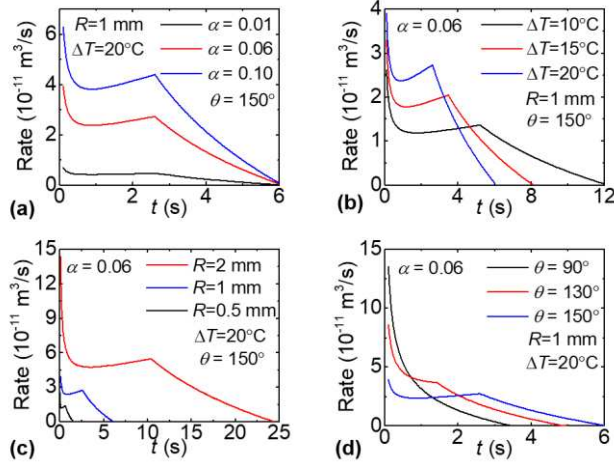


FIG. 4. Relations between bubble formation rate and (a) gas solubility,  $\alpha$ , (b) subcooled degree,  $\Delta T$ , (c) droplet curvature radius,  $R$ , (d) surface contact angle,  $\theta$ . When discussing one parameter's influence, other parameters are set constant.

To assess the bubble volume fraction in an ice droplet, we extracted the profiles of the water droplet and the ice droplet, as shown in Fig. 5(a), and then performed integrations along the  $y$ -axis to get the droplet volumes,  $V_{\text{water}}$  and  $V_{\text{ice}}$ . Thus, the bubble volume fraction in an ice droplet is equal to  $1 - V_{\text{water}}/\nu V_{\text{ice}}$ , where  $\nu$  is the density ratio of ice and water, which takes a value of 0.92. Figure 5(b) shows some results for the droplet icing on surfaces S1 and S2. The average value of bubble volume fraction is 6.10% with a standard deviation of 1.67%. That means that the ice droplet is actually a porous media rather than solid ice with a bubble volume fraction as high as 6%. This may change our previous perception, and may also bring some new changes in anti-icing/deicing techniques, such as more accurate assessment of ice quantity and ice adhesion.

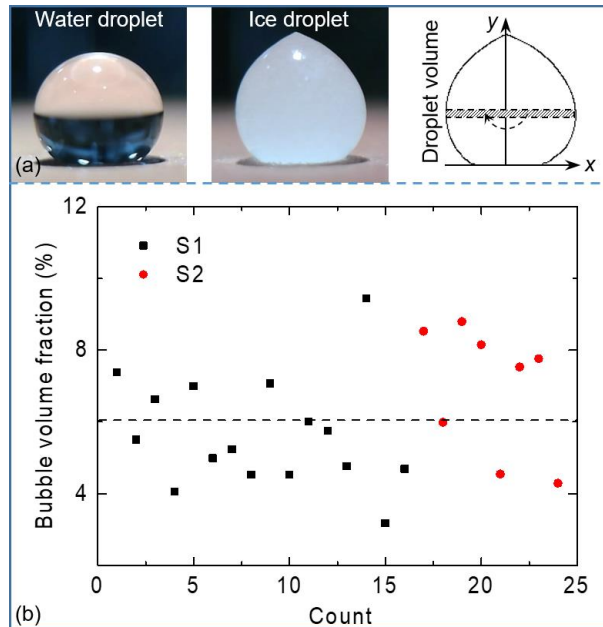


FIG. 5. (a) Calculation method of water droplet volume,  $V_{\text{water}}$ , and ice droplet volume,  $V_{\text{ice}}$ . The droplet profiles are extracted first and then integrations are performed along the  $y$ -axis to get the droplet volumes. The bubble volume fraction in an ice droplet is equal to  $1 - V_{\text{water}}/\nu V_{\text{ice}}$ , where  $\nu$  is the ratio of ice and water densities. (b) Bubble volume data in ice droplets on surfaces S1 and S2. The average value of bubble volume fraction is 6.10% with a standard deviation of 1.67%.

In summary, we demonstrated the bubble formation phenomenon in freezing droplets from micro-scale to millimeter scale, which lacks concern in previous literature. According to our measurements, the average value of bubble volume fraction in ice droplets is as high as 6%. Via a designed re-icing process, we clearly observed the bubbles are dissolved out from the ice front in an icing droplet, and then proposed a theoretical model coupled with the droplet icing physics. Based on the model, the bubble formation rate and its relationship with the main influencing factors (the gas solubility, the subcooled degree, the freezing time, the droplet size and the surface contact angle) were determined. This work may bring new perception that the ice droplet is actually a porous media rather than solid ice, and produce positive influence in related engineering fields such as anti-icing and deicing. However, about the bubble formation in icing droplets, this work is just the beginning; there are still many points to be concerned, such as bubble size, shape, distribution, etc.

This work is supported by the National Postdoctoral Program for Innovative Talents (No. BX20180024).

\*Corresponding author, d.wen@buaa.edu.cn

- [1] M. P. Fuller, A. M. Fuller, S. Kaniouras, J. Christophers, and T. Fredericks, *European Journal of Agronomy* **26**, 435 (2007).
- [2] F. T. Lynch and A. Khodadoust, *Progress in Aerospace Sciences* **37**, 669 (2001).
- [3] M. Rafati Nasr, M. Fauchoux, R. W. Besant, and C. J. Simonson, *Renewable and Sustainable Energy Reviews* **30**, 538 (2014).
- [4] S. Jung, M. K. Tiwari, N. V. Doan, and D. Poulikakos, *Nature communications* **3**, 615 (2012).
- [5] T. M. Schutzius, S. Jung, T. Maitra, P. Eberle, C. Antonini, C. Stamatopoulos, and D. Poulikakos, *Langmuir* **31**, 4807 (2015).
- [6] M. Schremb and C. Tropea, *Phys Rev E* **94**, 052804 (2016).
- [7] M. Tembely and A. Dolatabadi, *Journal of Fluid Mechanics* **859**, 566 (2018).
- [8] A. G. Marin, O. R. Enriquez, P. Brunet, P. Colinet, and J. H. Snoeijer, *Phys Rev Lett* **113**, 054301 (2014).
- [9] M. F. Ismail and P. R. Waghmare, *Applied Physics Letters* **109**, 234105 (2016).
- [10] S. Jung, M. K. Tiwari, and D. Poulikakos, *Proc Natl Acad Sci U S A* **109**, 16073 (2012).
- [11] S. Nath, C. E. Bisbano, P. Yue, and J. B. Boreyko, *Journal of Fluid Mechanics* **853**, 601 (2018).
- [12] T. M. Schutzius, S. Jung, T. Maitra, G. Graeber, M. Kohme, and D. Poulikakos, *Nature* **527**, 82 (2015).
- [13] E. Ghabache, C. Josserand, and T. Seon, *Phys Rev Lett* **117**, 074501 (2016).
- [14] S. Wildeman, S. Sterl, C. Sun, and D. Lohse, *Phys Rev Lett* **118**, 084101 (2017).
- [15] Y. Hou, M. Yu, Y. Shang, P. Zhou, R. Song, X. Xu, X. Chen, Z. Wang, and S. Yao, *Phys Rev Lett* **120**, 075902 (2018).
- [16] X. Sun and K. Rykaczewski, *ACS nano* **11**, 906 (2017).
- [17] F. Chu, X. Wu, and L. Wang, *ACS Appl Mater Interfaces* **9**, 8420 (2017).
- [18] K. Golovin, S. P. Kobaku, D. H. Lee, E. T. DiLoreto, J. M. Mabry, and A. Tuteja, *Sci Adv* **2**, e1501496 (2016).
- [19] Y. Wang, J. Xue, Q. Wang, Q. Chen, and J. Ding, *ACS Appl Mater Interfaces* **5**, 3370 (2013).
- [20] J. B. Boreyko and C. P. Collier, *ACS nano* **7**, 1618 (2013).
- [21] F. Chu, D. Wen, and X. Wu, *Langmuir* **34**, 14562 (2018).
- [22] Q. Zhang, M. He, J. Chen, J. Wang, Y. Song, and L. Jiang, *Chem Commun* **49**, 4516 (2013).
- [23] C. Madrazo, T. Tsuchiya, H. Sawano, and K. Koyanagi, *The Journal of the Society for Art and Science* **8**, 35 (2009).
- [24] J. Hruby and G. Kletetschka, *Journal of Glaciology*, 1 (2018).
- [25] F. Chu and X. Wu, *Appl. Surf. Sci.* **371**, 322 (2016).
- [26] F. Y. Lv and P. Zhang, *Appl. Surf. Sci.* **321**, 166 (2014).
- [27] J. Lv, Y. Song, L. Jiang, and J. Wang, *ACS nano* **8**, 3152 (2014).
- [28] F. Tavakoli and H. P. Kavehpour, *Langmuir* **31**, 2120 (2015).
- [29] L. Mishchenko, B. Hatton, V. Bahadur, J. A. Taylor, T. Krupenkin, and J. Aizenberg, *ACS nano* **4**, 7699 (2010).
- [30] X. Zhang, X. Wu, J. Min, and X. Liu, *Applied Thermal Engineering* **125**, 644 (2017).